

The effect of Non-centrosymmetry on optical and electronic properties of cubic BaHfO₃ perovskite structure

Tewodros Eyob,^{1, a)} Kenate Namera,^{1, b)} and Lemi Demeyu^{1, c)}

Department of Physics, Addis Ababa University, P.O. Box 1176, Addis Ababa, Ethiopia

(Dated: 18 February 2022)

The effect of Non-centrosymmetry on electronic and optical properties has been investigated using grid based projector augmented wave method code GPAW. The calculation of band gap using GLLB-SC which improves on the exchange potential and explicitly estimates the derivative discontinuity is similar to experimental result. Ferro-electricity of BaHfO₃ is increased as lattice distortion kept on increasing. Static dielectric constant, index of refraction only show slight change and in good agreement with experimental and other results. Absorption reaches highest peaks in visible frequency range, and absorption coefficient decreased as light goes through BaHfO₃ bulk, this in turn enhance excitonic property. Exciton binding energy increased over lattice distortion sites. The presented results are important in connection with development of typical perovskite optoelectronic device properties.

I. INTRODUCTION

Perovskite based materials have attracted much theoretical and experimental attention in recent years. Primarily, alkaline metal hafnate are of practical importance in numerous applications. These materials are best-known for their adaptability to exhibit several unique properties due to unstability to lower energy of structural distortions¹.

Cubic BaHfO₃ considered as ABO₃ perovskite oxides, where an A atom positioned at (0,0,0) corner of cube, a B atom at body center position(1/2, 1/2, 1/2), and three O atoms at face centered positions(1/2, 1/2, 0) forming a BO₆ regular octahedron²(see Fig.1). Several works

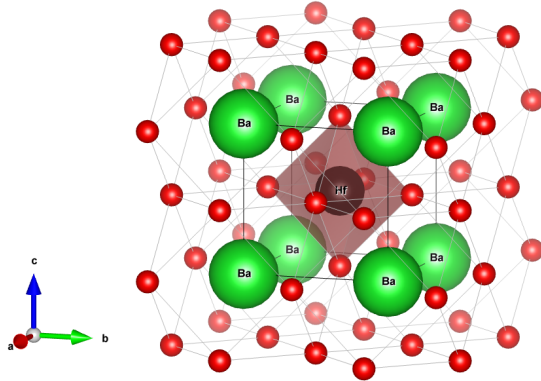


FIG. 1. Crystal structure of Cubic BaHfO₃ perovskites with octahedron of O₆ surrounding Hf atom.

have shown that the cubic phases of Pnma perovskites are unstable to both ferroelectric and octahedral rotation distortions³⁻⁶. In present work we follow different a

approach, and chose unique lattice displacement as distortions site in range of (3.85, 4.5) for slight change of centrosymmetry, and studied the effect on electronic, excitonic, ferroelectric and optical properties of BaHfO₃.

II. COMPUTATIONAL METHOD

We have implemented the Perdew-Burke-Ernzerhof(PBE) and Gritsenko, van Leeuwen, van Lenthe and Baerends potential(GLLB-SC) potentials to the grid-based projector augmented wave method code GPAW^{7,8} for Bandstructure calculations. It is a pseudopotential free approach, which allows more accurate and controlled description of electronic structure than the conventional pseudopotential approximations. For PAW core electrons the frozen-core approximation is used^{9,10}. Calculations were carried out self-consistently using GPAW PBE optimized lattice constant $a=4.225\text{\AA}$, Energy(E)=-36.147 eV, Bulk modulus(B)=157.939GPa(experimentally, $a=4.171\text{\AA}$), and a 8x8x8 k -points mesh over the entire BZ has been used. Each material is calculated in the framework of Density Functional Theory¹¹ using the GPAW code. All the proposed distortion sites are fully relaxed using the (PBE) functional¹².

III. RESULTS AND DISCUSSION

We considered lattice displacement of 0.05 increase in range of (3.85, 4.5) as distortion site for the slight shift of centrosymmetry. From Fig.2 it is clearly seen that highest polarization obtained at start, and gradually decreases till it comes to zero where barium hafnate's symmetry attained. Afterwards slow development of antiferroic property shown, this is because Hf atom, d-orbital from CB and p-orbital from VB contribution to Density of State(DOS) and non-centrosymmetry(lattice distortion) allows VB to have higher electron than CB and

^{a)}Electronic mail: tewodros.eyob@aau.edu.et

^{b)}Electronic mail: kenate.namera@gmail.com

^{c)}Electronic mail: lemi.demeyu@aau.edu.et

result in polarization. In second part, symmetry proportionates electron from VB to CB. Thus, no net electron spin state for polarization of perovskites. In similar manner, the first part of Fig.2 Hf atom, only p-orbital was contributing to VB, but in third part both p-orbital and s-orbital contributing to same band i.e CB. Therefore, Hf atom highly acted in reduction of net electron transfer from VB to CB, and resulted in almost zero ferroic property. However, at last Hf atom d-orbital and Ba, s-orbital contribution from CB is slightly greater than electron from VB. Hence, antiferroic property slowly grew up as distortion continued.

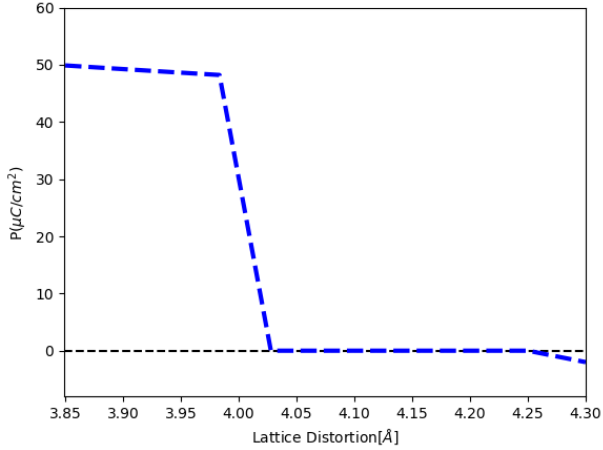


FIG. 2. Berry phase calculation of polarization ($\mu\text{C}/\text{cm}^2$) with respect to lattice distortion (\AA).

Here we presented representative sites and calculated the tolerance factor (t) which measures a geometric distortions of Perovskites¹⁴.

$$t = \frac{R_{A-O}}{\sqrt{2}R_{B-O}} \quad (1)$$

where R_{A-O} and R_{B-O} are the ideal $A-O$ and $B-O$ bond lengths for a particular ABO_3 material calculated using the bond valence model. Geometry relaxed for all representative lattice sites until the maximum ionic force less than $0.05(\text{eV}/\text{\AA})$. Table.I shows calculated bond length between Ba-O and Hf-O that determines symmetry of BaHfO_3 . At 3.85 site Hf-O bond pulled downward because of stronger force acted to shorten bond length and Ba-O bond pull upward in similar fashion, but at 4.171 and 4.2055 seems forces are in equilibrium, again Ba-O bond pulled upward, this chaotic disturbance introduce spontaneous polarization. Spontaneous polarization is an important property of ferroelectricity of materials, and obtained when crystal alters centrosymmetry¹⁵. Here we used BerryPhase Phase-Space Approach implemented in GPAW¹⁶ for the calculation of spontaneous polarization for representative sites shown in Fig.2.

TABLE I. Calculated minimum energy, Ba-O & Hf-O bond length and tolerance factor of representative lattice sites.

Sites(\AA)	Energy(eV)	Ba-O(\AA)	Hf-O(\AA)	Tolerance(t)
3.85	-35.17	4.69	1.95	1.70068
4.0277	-28.12	3.11	4.52	0.48653
4.171	-35.94	2.95	2.08	1.00287
4.2055	-36.07	2.96	2.10	0.99668
4.25	-36.06	5.17	2.12	1.72441

A. Electronic Properties

We investigated the electronic structure and respective density of state compared among selected sites. Our calculated band gap is about 4 eV, which is in good agreement to other theoretical results (3.9eV)¹⁷. As shown in Fig.3. Though fermi level oscillates in between band gap range, it does not affect the band gap size. However, distortion strongly affects the crystal symmetry and electronic structure of the cubic perovskite by stressing atomic orbitals, and confines mobility of electrons in either CB or VB, this situation leads to exhibit different electronic properties i.e ferroic, antiferroic, non-magnetic, P-type or N-type semiconductor so on. For band structure calculation we used an improved description of the GLLB-SC which improves on the exchange potential and explicitly estimates the derivative discontinuity^{18,19}. The GLLB-SC potential has been tested for cubic perovskites oxide systems with respect to experimental and G0W0 results giving an error below 0.5 eV. For all selected sites 3.85, 4.0277, 4.171, 4.2055 and respective fundamental gap in consecutive order is 6.164, 6.478, 6.55, 6.49 which only differ from experimental result by 0.5 eV.

B. Optical Properties

The optical properties can be gained from the complex dielectric function which is mainly connected with the electronic structure.

$$\epsilon(\omega) = \text{Re}\epsilon(\omega) + i\text{Im}\epsilon(\omega) \quad (2)$$

The imaginary part $\text{Im}\epsilon(\omega)$ is calculated from the electronic structure through the joint density of states²⁰ and the momentum matrix elements between the occupied and the unoccupied wave functions within the selection rules and is given by

$$\epsilon(\omega) = \frac{2e^2\pi}{\Omega\epsilon_0} \sum |\langle \psi_k^c | \hat{u}r | \psi_k^v \rangle|^2 \delta(E_k^c - E_k^v - E) \quad (3)$$

where e is the electronic charge, and ψ_k^c and ψ_k^v are the conduction band (CB) and valence band (VB) wave functions at k , respectively.

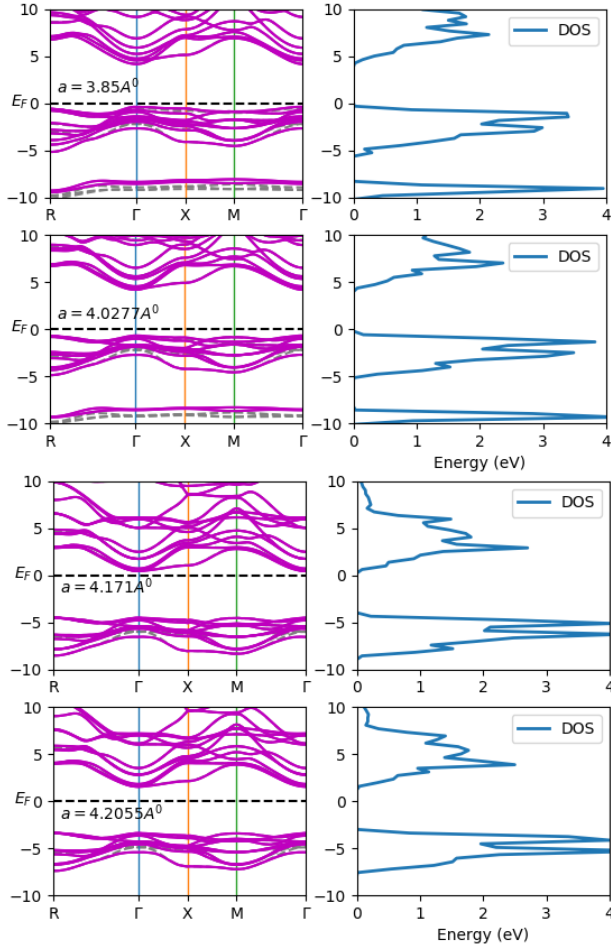


FIG. 3. Band structure and Fermi level change on lattice site 3.85, 4.171, 4.0277 and 4.2055 to their respective density of state.

The real part $\text{Re}\epsilon(\omega)$ can be extracted from the Kramer-Kronig relationship²¹. Other optical constants such as the refractive index $n(\omega)$, and absorption coefficient $I(\omega)$ can be computed from complex dielectric function $\epsilon(\omega)$ ²².

$$n(\omega) = \frac{1}{\sqrt{2}} \left\{ [\text{Re}\epsilon^2(\omega) + \text{Im}\epsilon^2(\omega)]^{1/2} + \text{Re}\epsilon^2(\omega) \right\}^{1/2} \quad (4)$$

and

$$I(\omega) = \frac{1}{\sqrt{2}} \frac{2\pi}{\lambda} \left\{ [\text{Re}\epsilon^2(\omega) + \text{Im}\epsilon^2(\omega)]^{1/2} - \text{Re}\epsilon^2(\omega) \right\}^{1/2} \quad (5)$$

The refractive index $n(\omega)$ and the dielectric function $\epsilon(\omega)$ of BaHfO₃ are shown in Fig.4 and compared in selected sites.

The overall behavior of $n(\omega)$ and static dielectric constants are found to be the same for all distortion sites and are in good agreement with other predicted study of $n(\omega)$ and dielectric constant²³. However, absorption peaks increased slightly as distortion goes far from cen-

trosymmetric point, and turns on excitonic effect.

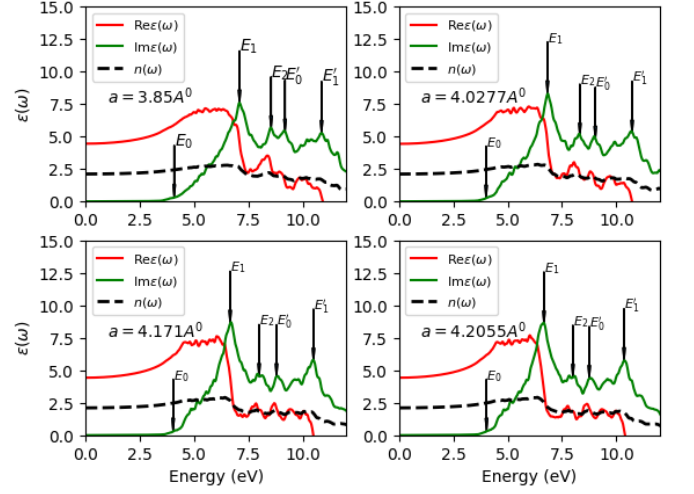


FIG. 4. The calculated real part $\text{Re}\epsilon(\omega)$ and imaginary part $\text{Im}\epsilon(\omega)$ of the dielectric $\epsilon(\omega)$ of BaHfO₃ at selected distortion sites.

The absorption coefficient $I(\omega)$ described as the amount of light absorbed per thickness of BaHfO₃ and calculated from Eq.(5). As illustrated in Fig.5 the absorption coefficient declines in the range of visible light(390-780nm) as distortion increases, and result in improved excitonic properties.

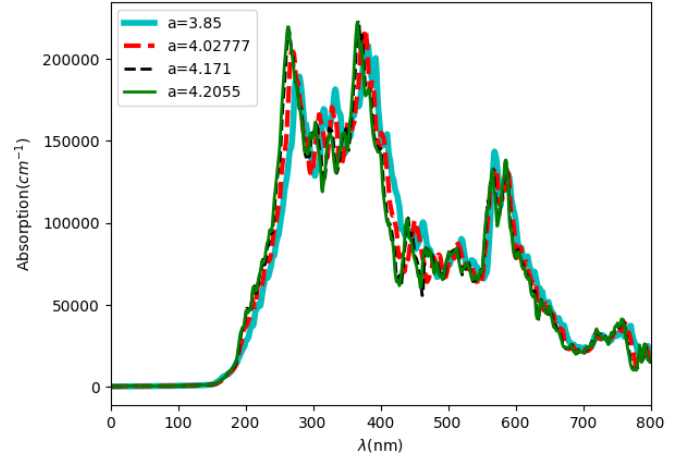


FIG. 5. The absorption coefficient $I(\omega)$ for BaHfO₃ at selected distortion sites.

The excitonic properties are very sensitive to the grid of \mathbf{k} -points used because the contributions of $\text{Im}\epsilon(\omega, \mathbf{q} \rightarrow 0)$ are very important. For the calculation of optical excitation we used Bethe-Salpeter Equation(BSE), and included a number of valence and conduction bands. The imaginary part of the dielectric function, which is directly related to absorption spectrum, can be calculated

by using the expression.

$$\text{Im}\epsilon(\omega)^{BSE} = \frac{16\pi^2 e^2}{\omega^2} \sum |e \cdot \langle 0 | v | s \rangle|^2 \sigma(\omega - \Omega^s) \quad (6)$$

The term $|e \cdot \langle 0 | v | s \rangle|$ is called the velocity matrix element in the direction of the polarization of the light e^{24} .

For the calculation of dielectric function 4 unoccupied bands have been proven sufficient in the energy range under consideration. A simple scissor shift of 0.8 eV is used to match the onset of the absorption to experiment, neglecting local field effects and the electron-hole correlation has been considered.

BaHfO₃ is known by a large fundamental gap which is obtained from GLLBSC calculation as 6.164, 6.478, 6.55, 6.49 in order of lattice distortion 3.85, 4.0277, 4.171 and 4.25. Note that the optical spectrum at Fig.6, the first excitonic peaks are at an energy of 6.236 eV, 6.0226 eV, 6.0016 eV and 6.00 eV, and the optical gap of BaHfO₃ in respective order of distortion sites are 3.85, 4.0277, 4.171 and 4.25, and also the G0W0 QP band gap are 4.01 eV, 4.2018 eV, 4.2779 eV, and 4.23 eV. Similarly, the excitonic binding energy are 1.99 eV, 1.8 eV, 1.72 eV, and 1.77 eV, respectively. We observe from Fig.6 that as the stronger BaHfO₃ absorption is the lower dielectric function resulting in reduced screen effect and higher exciton's binding energy and the longer lifetime. Therefore, reduced screening effect is because of lattice distortion sites.

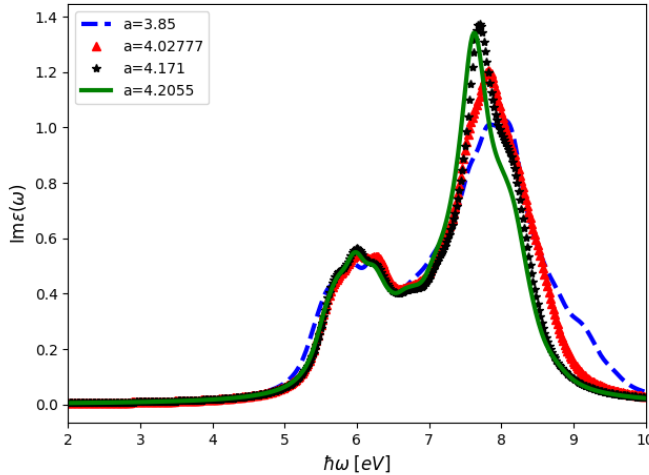


FIG. 6. The dielectric function of BaHfO₃ obtained from the BSE, without local field effect.

IV. SUMMARY

In this work, We have computed using Density Functional Theory, spontaneous polarization, electronic, and optical properties for representative values of lattice distortion. The calculated spontaneous polarization, elec-

tronic and optical spectra are in good agreement with experimental results. Efficiency of optoelectronic devices made of BaHfO₃ material should consider distortion effect on exciton binding energy as per increase in absorption spectrum and decrease in absorption coefficient. Ferroic property of B-sites of ABO₃ system is highly affected by tolerance factor which measures distortion of perovskites.

ACKNOWLEDGMENTS

Addis Ababa University Physics Department and International Science Program, Uppsala University, Sweden are gratefully acknowledged for providing computational facilities. The authors are grateful to Prof. P. Singh, Addis Ababa University for helpful discussion.

- ¹ Benrekia, A.R., Benkhetto, N., Nassour, A., Driz, M., Sahnoun, M., & Lebe'gue, S. (2012). Structural, electronic and optical properties of cubic SrTiO₃ and KTaO₃: Ab initio and GW calculations. *Physica B, Condensed Matter*, **407**(13), 2632-2636. <http://dx.doi.org/10.1016/j.physb.2012.04.013>.
- ² S. Amisi (2019). First-principles study of structural and vibrational properties of SrHfO₃ compared to SrZrO₃. *Computational Condensed Matter* **20** e00383, <https://doi.org/10.1016/j.cocom.2019.e00383>.
- ³ D.P. Rai et al (2017). Electronic and optical properties of cubic SrHfO₃ at different pressures: A first principles study, *Materials Chemistry and Physics* **186**, 620e626, <http://dx.doi.org/10.1016/j.matchemphys.2016.11.045>.
- ⁴ Syed Muhammad Alay-e-Abbas, Safdar Nazir, Naveed Ahmed Noor, Nasir Amin, and Ali Shaukat (2014). Thermodynamic Stability and Vacancy Defect Formation Energies in SrHfO₃, *The Journal of Physical Chemistry C* **118**(34), 19625-19634, <http://dx.doi.org/10.1021/jp506263g>.
- ⁵ R.B. Behram et al (2016). Theoretical investigation of mechanical, optoelectronic and thermoelectric properties of BiGaO₃ and BiInO₃ compounds *Materials Science in Semiconductor Processing* **41**, 297-303, <http://dx.doi.org/10.1016/j.mssp.2015.09.010>.
- ⁶ Francis Opoku et al (2017). Enhancing Charge Separation and Photocatalytic Activity of Cubic SrTiO₃ with Perovskite-Type Materials MTaO₃ (M = Na, K) for Environmental Remediation: A First-Principles Study, *ChemistrySelect*, **2**, 6304-6316, <http://dx.doi.org/10.1002/slct.201700886>.
- ⁷ J Enkovaara et al (2010). Electronic structure calculations with GPAW: a real-space implementation of the projector augmented-wave method. *J. Phys.: Condens. Matter* **22**, 253202, <https://doi.org/10.1088/0953-8984/22/25/253202>.
- ⁸ Mortensen, J. J. and Hansen, L. B. and Jacobsen, K (2015). W. Real-space grid implementation of the projector augmented wave method. *Phys. Rev. B*, **71**:035109, <https://doi.org/10.1103/PhysRevB.71.035109>.
- ⁹ P. E. Blöchl (1994). Projector augmented-wave method. *Phys. Rev. B* **50**, 17953, <https://doi.org/10.1103/PhysRevB.50.17953>.
- ¹⁰ Kresse, G. & Joubert, Daniel (1999). From Ultrasoft Pseudopotentials to the Projector Augmented-Wave Method. *Phys. Rev. B*, **59**, 1758. <http://dx.doi.org/10.1103/PhysRevB.59.1758>.
- ¹¹ C. Fiolhais, F. Nogueira, and M. Margues, editors (2003). *A Primer in Density Functional Theory*, volume **620** of *Lecture Notes in Physics*. Springer, <http://dx.doi.org/10.1007/3-540-37072-2>.
- ¹² Ernzerhof, Matthias & Scuseria, Gustavo (1999). Assessment of the Perdew-Burke-Ernzerhof exchange-correlation functional.

- The Journal of Chemical Physics. **110**, <http://dx.doi.org/10.1063/1.478401>.
- ¹³Miru, Noh & Soonchul, Choi & Dongjae, Lee & Minhyun, Cho & Changhyun, Jeon & Yunsang, Lee. (2013). Structural and Optical Properties of AZrO₃ and AHfO₃ (A = Ca, Sr, and Ba). New Physics: Sae Mulli. **63**, 939, <http://dx.doi.org/10.3938/NPSM.63.939>.
 - ¹⁴Nicole A. Benedek Craig J. Fennie (2013). Why Are There So Few Perovskite Ferroelectrics? J. Phys. Chem. C 2013 117 2613339-13349, <https://doi.org/10.1021/jp402046t>.
 - ¹⁵Perdew, J.P., Burke, K., Ernzerhof, M. (1996). Generalized gradient approximation made simple. Phys. Rev. Lett. **77**, 3865-3868, <https://doi.org/10.1103/PhysRevLett.77.3865>.
 - ¹⁶Chrusciński, Dariusz (2006). Phase-Space Approach to Berry Phases, Open Systems & Information Dynamics, **13**, 1, 67-74, <https://doi.org/10.1007/s11080-006-7268-3>.
 - ¹⁷C. Azahaf et al. (2015). Theoretical investigation of spontaneous polarization, electronic and optical properties of cubic perovskite BaHfO₃, Optical & Quantum Electronics, **47**, 8, p2889-2897. <https://doi.org/10.1007/s11082-015-0178-2>.
 - ¹⁸O. Gritsenko, R. van Leeuwen, E. van Lenthe and E. J. Baerends (1995). Self-consistent approximation to the Kohn-Sham exchange potential. Physical Review A, **51**, 1944, <https://doi.org/10.1103/PhysRevA.51.1944>.
 - ¹⁹M. Kuisma, J. Ojanen, J. Enkovaara and T. T. Rantala (2010). Kohn-Sham potential with discontinuity for band gap materials. Physical Review B, **82**, 115106, <https://doi.org/10.1103/PhysRevB.82.115106>.
 - ²⁰M. Gajdoš, K. Hummer, G. Kresse, J. Furthmüller, and F. Bechstedt (2006). Linear optical properties in the projector-augmented wave methodology, Phys. Rev. B **73**, 045112, <https://doi.org/10.1103/PhysRevB.73.045112>.
 - ²¹S. Saha, T. P. Sinha, and A. Mookerjee (2000). Electronic structure, chemical bonding, and optical properties of paraelectric BaTiO₃, Phys. Rev. B **62**, 8828-8834, <https://doi.org/10.1103/PhysRevB.62.8828>.
 - ²²C. Samantaray, H. Sim, and H. Hwang (2005). First-principles study of electronic structure and optical properties of barium strontium titanates (Ba_xSr_{1-x}TiO₃), Appl. Surf. Sci. **250**, 146-151, <https://doi.org/10.1063/1.5047094>.
 - ²³M. Gajdoš, K. Hummer, and G. Kresse (2006). Linear optical properties in the projector-augmented wave methodology, Phys. Rev. B **73**, 045112, <https://doi.org/10.1103/PhysRevB.73.045112>.
 - ²⁴F. Ferreira and R. M. Ribeiro (2017). Improvements in the GW and Bethe-Salpeter-equation calculations on phosphorene, Phys. Rev. B **96**, 115431, <https://doi.org/10.1103/PhysRevB.96.115431>.